Metabolic Engineering 13 (2011) 38–48

Contents lists available at ScienceDirect

Metabolic Engineering

journal homepage: www.elsevier.com/locate/ymben

Synergy between ^{13}C-metabolic flux analysis and flux balance analysis for understanding metabolic adaption to anaerobiosis in *E. coli*

Xuewen Chen [a,*], Ana P. Alonso [a], Doug K. Allen [b], Jennifer L. Reed [c], Yair Shachar-Hill [a]

[a] Department of Plant Biology, Great Lakes Bioenergy Research Center, Michigan State University, East Lansing, MI 48824, United States
[b] USDA ARS, Plant Genetics Research Unit, Donald Danforth Plant Science Center, St. Louis, MO 63132, United States
[c] Chemical and Biological Engineering Department and Great Lakes Bioenergy Research Center, University of Wisconsin-Madison, Madison, WI 53706, United States

ARTICLE INFO

Article history:
Received 29 April 2010
Received in revised form
20 October 2010
Accepted 16 November 2010
Available online 1 December 2010

Keywords:
E. coli
Metabolic flux analysis
Flux balance analysis
Maintenance ATP utilization
Formate hydrogen lyase
Incomplete TCA cycle

ABSTRACT

Genome-based Flux Balance Analysis (FBA) and steady-state isotopic-labeling-based Metabolic Flux Analysis (MFA) are complimentary approaches to predicting and measuring the operation and regulation of metabolic networks. Here, genome-derived models of *Escherichia coli* (*E. coli*) metabolism were used for FBA and ^{13}C-MFA analyses of aerobic and anaerobic growths of wild-type *E. coli* (K-12 MG1655) cells. Validated MFA flux maps reveal that the fraction of maintenance ATP consumption in total ATP production is about 14% higher under anaerobic (51.1%) than aerobic conditions (37.2%). FBA revealed that an increased ATP utilization is consumed by ATP synthase to secrete protons from fermentation. The TCA cycle is shown to be incomplete in aerobically growing cells and submaximal growth is due to limited oxidative phosphorylation. An FBA was successful in predicting product secretion rates in aerobic culture if both glucose and oxygen uptake measurement were constrained, but the most-frequently predicted values of internal fluxes yielded from sampling the feasible space differ substantially from MFA-derived fluxes.

1. Introduction

The metabolic fluxome is one of the most direct descriptions of metabolic network operation (Lee et al., 1999; Ratcliffe and Shachar-Hill, 2006; Sauer, 2006; Tang et al., 2009; Wiechert, 2001; Wiechert et al., 2007; Wittmann, 2002). Quantifying the fluxome and the structure and potential of the metabolic network through which it flows are therefore important goals in systems biology in the rational engineering of industrial microbes (Boghigian et al., 2010; Fong et al., 2005; Kim et al., 2008; Koffas and Stephanopoulos, 2005; Liao and Oh, 1999; Meadows et al., 2010; Stephanopoulos, 1999). Several experimental and theoretical toolsets have been used to measure the fluxome and to analyze metabolic networks, their capabilities, performance and regulation and to predict and understand the effects of genetic changes (Antoniewicz et al., 2007a; Becker et al., 2007; Bordel and Nielsen, 2010; Feist et al., 2009; Price et al., 2004; Sauer, 2006; Sauer et al., 1999; Schmidt et al., 1997; Suthers et al., 2010; Wiechert, 2002; Wiechert and de Graaf, 1997; Wiechert et al., 2001; Wittmann, 2002; Zamboni et al., 2005). Two of the most successful approaches, constraint-based and metabolic flux analysis, both focus on metabolic steady-state (where the fluxes are constant) and employ modeling methods.

Constraint-based models use a stoichiometric approach to study the fluxome of metabolic networks, in which all possible net flux distributions (feasible flux space) are constrained by observed cellular input and output measurements (external fluxes) and by mass balance and thermodynamic equations (Price et al., 2004). Flux balance analysis (FBA) probes this solution space to identify metabolic flux distributions that optimize certain objectives (usually maximizing growth). This and other constraint-based methods have been successfully used to predict growth and by-product secretion of microbes (Fong et al., 2005; Park et al., 2007; Segre et al., 2002; Varma and Palsson, 1994). One common challenge in interpreting FBA results is the existence of multiple optimal intracellular fluxes that meet the objective equally well. Therefore, the intracellular fluxes within the metabolic network (internal fluxes) have been studied mostly from the properties of the optimal solution space (Khannapho et al., 2008; Mahadevan and Schilling, 2003; Reed and Palsson, 2004), or by an arbitrary choice of optimal flux distributions (Papp et al., 2004; Segre et al., 2002).

Isotopic steady-state metabolic flux analysis (MFA) is an experimentally based method of obtaining internal carbon and energy fluxes, by tracking atom rearrangements that are measured in labeling experiments(Antoniewicz et al., 2007a; Nanchen et al., 2007; Sauer et al., 1999; Schmidt et al., 1997; Wiechert and de Graaf, 1997; Wiechert et al., 1997; Wittmann, 2002; Zamboni et al., 2009; Zamboni et al., 2005). Labeled substrates are supplied to

* Corresponding author. Fax: +1 517 353 1926.
E-mail address: xwchen@msu.edu (X. Chen).

1096-7176/$ - see front matter © 2010 Elsevier Inc. All rights reserved.
doi:10.1016/j.ymben.2010.11.004

cells, and the labeling of metabolic end-products, including biomass components, is obtained by analytical chemical techniques. Fluxes are estimated by optimized fitting of internal fluxes to the measurements of labeling and external fluxes. The resulting flux maps quantitatively describe flow through metabolism. Results from an MFA also include estimates of the forward and reverse rates through reversible reactions in the form of exchange flux estimates. Exchange fluxes report on substrate cycling and are therefore important to understand metabolic efficiency and regulation. However, since carbon labeling measurements are used, MFA can only describe the metabolic activities related to carbon flow and ignores non-carbon metabolism and transport.

MFA and FBA are thus inherently complementary in describing fluxes through metabolism, and the combination of both is likely to provide greater insights into evolution and behavior of metabolic networks. Some comparisons between MFA and FBA findings have been reported. Segre et al. (2002) and Shlomi et al. (2005) developed novel minimization of metabolic adjustment (MOMA) and regulatory on/off minimization (ROOM) methods to predict metabolic response to genetic perturbations of *E. coli* and yeast. The MOMA and ROOM solutions based on genome-scale FBA optimal solutions were compared with an MFA determined flux maps in earlier studies (Emmerling et al., 2002; Hua et al., 2003; Jiao et al., 2003; Peng et al., 2004). Schuetz et al. evaluated different objective functions for predicting intracellular fluxes of an *E. coli* model containing 98 reactions. The biologically meaningful objective functions were identified by comparing the optimal solutions with ^{13}C based metabolic flux ratios. However to our knowledge, no studies have reported genome-scale FBA modeling and ^{13}C-MFA of the same system under the same conditions and using the same structural network model. Applied to a model system, this would allow a direct detailed comparison of the fluxes derived by the two approaches and an exploration of their synergistic capability to enhance our understanding of microbial physiology.

E. coli is a model organism for studying metabolism and it has been used to establish and test a wide range of biochemical and flux analysis tools. The ability to grow in the presence or absence of oxygen also makes these cells a model organism for studying growth under conditions which are important for biotechnology and bioenergy applications (Kim et al., 2009; Lin and Tanaka, 2006). Here a ^{13}C-MFA network model was generated for *E. coli* based on a previous genome-scale constraint-based model (Reed et al., 2003). This includes a complete description of all carbon rearrangements in *E. coli* central metabolism. The ^{13}C-labeling of proteinogenic amino acids and intracellular metabolic intermediates after growth in labeled medium as well as substrate uptake and product secretion rates were determined using GC and LC mass spectrometry, NMR spectroscopy, enzymatic assays and gas analysis methods. Labeling and external flux measurements were performed with wild-type *E. coli* (K-12 MG1655) cultured in M9 minimal medium supplemented with glucose as sole carbon and energy source under aerobic and fermentative conditions. The resulting MFA maps were compared with results from FBA using a genome-scale constraint-based metabolic model (iJR904) (Reed et al., 2003) to test the accuracy of FBA external flux predictions, assess an FBA based internal flux predictions, and evaluate metabolic optimality and efficiency of an ATP usage by *E. coli* during growth in the absence and presence of oxygen.

2. Materials and method

2.1. Bacterial strain, growth medium and culture conditions

E. coli K-12 MG1655 was purchased from American Type Culture Collection (Manassas, VA, ATCC number: 47076). Cells were grown in defined minimal medium (M9) with glucose (2 g/l throughout) as the sole carbon source (Sambrook and Russel, 2001). Both aerobic and anaerobic cultures were incubated at 37 °C and 250 rpm in a Labnet 311 DS Digital incubator. Cell growth was measured using a spectrophotometer (Beckman DU 800, Fullerton, CA). Cells were harvested at middle log-phase by centrifugation at 2000*g* and 4 °C.

In ^{13}C-labeling experiments, the glucose used was 20% (mol/mol) U–^{13}C glucose and 80% (mol/mol) [1–^{13}C] glucose (Sigma). ^{1}H and ^{13}C NMR were used to directly validate the purity of glucose in the medium of the same experiments, in which cells were harvested for MFA. C_1 labeling of glucose was $98.8 \pm 0.6\%$ for aerobic media and $98.7 \pm 1.1\%$ in anaerobic media. C_6 labeling of glucose was $20.4 \pm 0.4\%$ for aerobic media and $19.9 \pm 0.5\%$ in anaerobic media. Isotopic steady-state was confirmed for OD_{600} values between 0.40 and 0.80 for aerobic culture and between 0.25 and 0.46 for anaerobic culture by analyzing the labeling of amino acids (data not shown).

2.1.1. Aerobic culture

For growth rate, labeling and substrate uptake/product secretion, analyses of aerobic cultures, cells were precultured overnight in 30 ml M9 medium containing unlabeled glucose in 250 ml Bellco triple baffled shake flasks. Experimental cultures were started at $OD_{600} \approx 0.01$ by transferring around 200 μl preculture to 30 ml fresh medium containing labeled glucose. Cells were harvested at the middle of log-phase ($OD_{600} \approx 0.7$).

An O_2-enhanced experiment was performed in PYREX Erlenmeyer flasks sealed with gas impermeable septum caps. Cells were cultured in 30 ml medium in the flask with 35% O_2 in the headspace. Growth was monitored between OD600 values of 0.02 and 1.0. The headspace was 255 ml and the amount of O_2 consumed was measured by gas analysis of the headspace and was $< 10\%$ of the initial amount in the enhanced O_2 experiments; the level of O_2 remained substantially higher than the level present in air throughout the whole culture period.

2.1.2. Anaerobic culture

For growth rate, labeling and substrate uptake/product secretion, analyses of anaerobic cultures, 250 ml PYREX Erlenmeyer flasks each containing 30 ml M9 medium were sealed with septum caps and flushed with N_2 for 30 min. Anaerobic conditions in the headspace were confirmed by measuring O_2 content using paramagnetic response gas analysis. Around 700 μl cells were transferred to the flask by injection through the septum after anaerobic conditions were established. Cells were precultured overnight under anaerobic conditions in M9 media with unlabeled glucose. Experimental cultures started at $OD_{600} \approx 0.01$ and were harvested at the middle of the log-phase ($OD_{600} \approx 0.4$).

2.2. Determination of substrate uptake and product secretion

Cells were harvested by centrifuging at 2000*g* and 4 °C. Cultured medium was sterilized by passing through a 0.22 μm filter. The concentrations of the uptake substrate and secreted products (glucose, acetate, ethanol, formate and succinate) were measured in 30 ml culture using commercial enzyme assay kits according to the manufacturer's instructions (R-Biopharm, Inc., Marshal, MI) and by NMR (succinate and lactate) from fully relaxed ^{1}H NMR spectra of lyophilized culture medium resuspended in D_2O—using methyl-phosphonic acid as an internal standard. O_2 uptake and CO_2 secretion rates were measured by paramagnetic response and infrared gas analysis using, respectively, a paramagnetic O_2 detector (Series 1100, Servomex Co., http://www.servomex.com/) and an infrared CO_2 detector (ADC 255-MK3, Analytical Development Co.) (Goffman et al., 2005). To measure an O_2 uptake and CO_2 secretion

rates in the aerobic cultures, cells were inoculated aerobically into a 250 ml PYREX Erlenmeyer flask with 120 ml medium. The flask was sealed with septum cap between OD_{600} of 0.55 and 0.83. Gas samples at different time points were collected when the flasks were sealed. For the anaerobic culture, cells were inoculated anaerobically in 250 ml PYREX Erlenmeyer flask with 150 ml medium and gas samples were collected between OD_{600} 0.16 and 0.42.

Substrate uptake rates and production secretion rates were calculated using the equation (Sauer et al., 1999)

$$v = \frac{C(t_2) - C(t_1)}{(\mathrm{OD}(t_2) - \mathrm{OD}(t_1))f}\mu,$$

where $C(t)$ and $\mathrm{OD}(t)$ are the extracelluar metabolite concentrations and OD_{600} at time t; μ is the growth rate of the culture; and f is the conversion coefficient between OD_{600} and biomass dry weight per unit volume of media. We determined the conversion coefficient f to be 0.42 ± 0.03 g dry weight/liter medium/OD_{600} for aerobic culture and 0.59 ± 0.02 g dry weight/liter medium/OD_{600}.

2.3. GC–MS analysis of amino acids

Amino acid sample preparation was based on previously reported methods (Nanchen et al., 2007; Schwender et al., 2003). Cells were washed twice with 0.9% NaCl, resuspended in 6 N HCl at 110 °C for 24 h, and dried under a stream of N_2 at 60 °C to remove HCl. Samples were re-dissolved in 0.1 N HCl, passed through 0.2 μm filter twice to remove cellular debris and dried under an N_2 stream and 60 °C. Amino acids were derivatized using *N*-Methyl-*N*-[tert-butyldimethyl-silyl]trifluoroacetimide (MTBSTFA, Sigma Aldrich) as reported by Allen et al. (2007) and Schwender et al. (2003). GC–MS analysis was performed on an Agilent 5973 inert MSD benchtop quadrapole mass spectrometer as previously described (Allen et al., 2007; Schwender et al., 2003). GC–MS signals were corrected for natural abundance of O, N, H, Si and S in the derivative parts of the molecules (Schwender et al., 2003).

We selected the fragments suitable for ^{13}C-MFA reported by Allen et al. (2007). We ran amino acid standards, corrected for natural abundance and compared these with theoretical values (Table S5). All selected fragment standards corrected to within 1% of theoretical values.

2.4. NMR analysis of secreted products

^{1}H and ^{13}C NMR analyses were used to measure the labeling and concentration of secreted metabolites. Of about 15 ml of cell culture was centrifuged to obtain the supernatant for an NMR analysis. The pH of the supernatant was increased to about 9 by addition of 500 mM NH_4OH. The samples were lyophilized and re-dissolved in 0.7 ml D_2O. ^{1}H NMR and ^{13}C NMR analyses were performed on Varian Unity 500 and Inova 600 instruments, respectively, with 5 mm probes. ^{1}H NMR spectra were obtained at 499.74 MHz with a pulse of 6 μs. An acquisition time of 4 s was used, followed by a recycle delay of 1 s. ^{13}C NMR spectra were performed at 150.84 mHz with a pulse of 6 μs. An acquisition time was set to 1.3 s, and a recycle delay was set to 80 s to allow full relaxation of carboxylate groups. Compounds were identified using Spectral Database for Biological Compounds (http://riodb01.ibase.aist.go.jp/sdbs/cgi-bin/direct_frame_top.cgi) and Biological Magnetic Resonance Data Bank (http://www.bmrb.wisc.edu/). The enrichment of ^{13}C was determined as previously described (Dieuaide-Noubhani et al., 1995; Ratcliffe and Shachar-Hill, 2006; Rontein et al., 2002).

2.5. LC–MS/MS analysis of intracellular metabolites

The liquid chromatography was performed with an ACQUITY UPLC® pump system (Waters). Samples in the autosampler were kept at 4 °C, whereas the liquid chromatography analysis was carried out at room temperature. Phosphorylated metabolites were separated by an ion chromatography on an IonPac® AS11 (250 mm × 2 mm, Dionex) column equipped with a guard column AG11 (50 mm × 2 mm, Dionex) at a flow rate of 0.35 mL min^{-1}, as previously described by Alonso et al. (2010). The MS/MS analyses were performed with a Quattro-PremierTM (Waters), triple quadrupole mass spectrometer. Mass spectra were acquired using electrospray ionization in negative ion mode, using multiple reaction monitoring. The capillary voltage, extractor voltage and rf lens setting were set at 3.00 kV, 5 V and 0.0, respectively. The flow rates of cone gas and desolvation gas were 50 and 800 L h^{-1}, respectively. The source temperature and desolvation temperature were 100 and 350 °C, respectively. The $[M-H]^{-1}$ were fragmented by collision-induced dissociation with argon as the collision gas at a manifold pressure of 2.67×10^{-3} mbar. Collision energies and source cone potentials, optimized for each transition using Waters QuanOptimize software, were found to be, respectively, 25 V and 15 eV for Glc6P and Fru6P, (Alonso et al., 2010), 3 V and 22 eV for 2PG or 3PG, and 10 V and 16 eV for PEP. The selected daughter ions are $[H_2PO_4]^-$ (m/z=97) for Glc6P, Fru6P and 2 or 3PG, and $[PO_3]^-$ (m/z=79) for PEP. For a phosphorylated metabolite containing n atoms of carbon, we follow n+1 transitions: $[M_0-H]^-$/97, $[M_{+1}-H]^-$/97, …, $[M_{+n}-H]^-$/97. Data were acquired with the MassLynx 4.0 software and processed for calibration and for quantification of the analytes with QuanLynx software (Waters). For the sampling, 15 mL of *E. coli* suspension culture (approximately OD_{600}=0.6 and 0.3 for aerobic and anaerobic cultures, respectively) were quickly filtered through a nylon membrane filter (Whatman®, 0.45 μm pore size and 47 mm diameter), and the cells retained on the filter were rinsed with 15 mL of 2.6% NaCl (Bolten et al., 2007). The filter was then transferred to a test tube and frozen in liquid N_2. Intracellular metabolites were extracted using boiling water [as previously described by Alonso et al. (2010)]. Dried extracts were resuspended in 100 μL of Milli-Q water to be analyzed by LC–MS/MS.

2.6. Flux balance analysis

The expanded genome-scale constraint-based stoichiometric model of *E. coli* K-12 (iJR904 GSM/GPR) developed by Reed et al. (2003) was used for FBA. The model was developed for *E. coli* K-12 MG1655 and included 931 unique biochemical reactions. FBA simulations were performed using the Cobra Tool Box 1.3.3 (Becker et al., 2007) in MATLAB. The uptake rates of glucose and/or O_2 were/was used in the FBA analysis to predict external secretion rates and internal net fluxes. Maximizing cellular growth rate was used as the objective function for all FBA simulations. Robustness analysis (Edwards and Palsson, 2000) was used to predict product secretion, substrate uptake and ATP synthase rates as functions of growth rate. Flux variability analysis (FVA) (Mahadevan and Schilling, 2003) was used to predict the range over which internal fluxes can vary, while still maintaining the maximal growth rate. The distribution of individual internal flux distributions in the range defined by an FVA was estimated by uniform random sampling of metabolic solution space, using the Cobra toolbox (Becker et al., 2007).

2.7. Construction and modeling of the MFA ^{13}C isotopic network

A MFA isotopic network of wildtype *E. coli* K-12 MG1655 was constructed by simplifying the genome-scale metabolic model and

mapping carbon atoms in reactants to products (Reed et al., 2003). The goal of model simplification is to reduce the number of metabolites that are accounted for (which reduces the number of variables in the MFA model) while keeping intact the carbon flow in the network. Strategies used in simplification include pooling of metabolites that are rapidly and reversibly interconverted, collapsing multiple irreversible steps of linear pathways into single reactions, and grouping metabolites with the same carbon skeleton and non-differential carbon labeling (Ratcliffe and Shachar-Hill, 2006). The resulting ^{13}C isotopic MFA network (Table S4 in Supplemental materials) includes the full central metabolic network and amino acid and nucleotide biosynthesis.

2.8. ^{13}C-metabolic flux analysis

We incorporated measured external fluxes, labeling measurement and a literature-derived biomass composition (Neidhardt and Edwin Umbarger, 1996) into the MFA ^{13}C-network to identify internal fluxes in metabolism. All external fluxes in Table 1, except O_2 and CO_2, were used in an MFA. The formate and ethanol secretion rates measured are underestimates of real rates due to evaporation, and were therefore used to set the lower bounds for these external fluxes in both MFA and FBA simulations. Labeling measurements of amino acids by GC–MS and of secreted acetate and lactate (by an NMR) were also included in an MFA. Since ~98% of the biomass was made during the labeling period, GC–MS data were corrected for an unlabeled biomass. The biomass composition was converted to production rates of individual biomass components, and was incorporated into the simulations.

2.9. Optimization and statistics

The ^{13}C isotopic network model was implemented in the ^{13}C-FLUX software to obtain detailed maps of carbon and energy flow through metabolism (Wiechert et al., 2001). Given a set of starting initial fluxes, the ^{13}C-Flux software searches the feasible solution space of an isotopic network for a solution that best fits the labeling and flux measurements (minimizing the sum of squared residuals weighted by the standard deviation of each measurement (SS_{res})). Multiple sets of initial fluxes are necessary to avoid finding only local minima in the search. Here, around 700 initial flux sets were generated by sampling the feasible solution space. The initial fluxes were supplied to ^{13}C-flux software to start independent simulations.

The simulations were performed in parallel on a SGI 1024-core cluster of 128 nodes (2 quad-core Xeons at 2.3 GHz, 8 GB of memory and 250 GB of local disk per node) at the High Performance Computing Center, Michigan State University. The automation of this process was implemented in Perl by Dr. Hart Poskar (Plant Biology Department, Michigan State University). The distribution of SS_{res} from about 700 simulations was shown in Supplementary Materials (Fig. S4). The global SS_{res} is 86.6 for an aerobic fitting that used 153 measurements and 283.6 for an anaerobic fitting that used 157 measurements. A correlation plot of the measurement constraints used in fitting and model predicted results was shown in Fig. S5. A statistical analysis was performed using the EstimateStat tool in ^{13}C-flux to provide confidence intervals for each flux.

Although all labeling experiments had at least three biological replicates, the standard deviation of most GC–MS signals was $<1\%$ which may overly state the accuracy of these results and give unreasonable flux estimation by overly constraining particular parameters. We estimated the accuracy of our labeling measurements to be 0.5%, which was typically larger than the biological replicate standard deviation. We therefore increased the biological replicate standard deviation of GC–MS data by 0.5% (Table S5). Deviation of glucose uptake, substrate secretion and NMR labeling measurements were established from the biological replicates. A biomass composition of *E. coli* B/r from the literature (Neidhardt and Edwin Umbarger, 1996) was used to estimate effluxes of biomass production in the MG1655 strain. Most calculated biomass effluxes are less than 1% of glucose uptake rate. An error of 50% was used for the effluxes in an MFA, because this reflects a reasonable error for these small measured values.

A confidence interval of each optimized flux was obtained from a method based on least squares approach (Wiechert et al., 1997), and was determined from multiple experiments (biological variations, $n \geq 3$). The resulted flux maps, optimized net fluxes and forward/backward fluxes of reversible reactions are shown in Fig. 1, Table 2 and Fig. S1 (Supplemental materials).

3. Results

3.1. Growth parameters and uptake/secretion rates

The measured growth parameters and uptake/secretion fluxes are shown in Table 1. During an anaerobic growth, the glucose uptake and acetate secretion increased by ~70% and ~31%, respectively, as compared to an aerobic growth. No lactate, succinate, formate or ethanol were detected in the aerobic culture medium by either enzyme assay or ^{1}H NMR. We measured CO_2 level in the anaerobic culture and did not find a significant buildup of CO_2 in sealed flasks. This is because formate instead of CO_2 is produced from pyruvate in fermentation to reduce production of NADH. CO_2 released from pentose phosphate pathway, TCA cycle and biomass synthesis is refixed by phosphoenolpyruvate carboxylase through anaplerotic pathway. These growth rates and external fluxes are consistent with literature reports (Fischer et al., 2004; Hua et al., 2006; Neidhardt, 1996; Nicolas et al., 2007).

3.2. ^{13}C-metabolic flux maps

Aerobic and anaerobic ^{13}C-flux maps are shown in Fig. 1 and Table 2 for central metabolism, and the supplementary materials contain the detailed biosynthetic fluxes. Neither the aerobic nor anaerobic flux map shows significant rates of substrate cycling (Table 2). The aerobic flux map (Fig. 1A) is characterized by significant carbon flows through glycolysis and the oxidative pentose phosphate pathway (OPPP). About 27% of glucose taken up was directed to the OPPP through glucose-6-phosphate dehydrogenase (G6PDH2r). Carbon flow through citrate synthase (CS) and aconitase (ACONT) in TCA accounts for 16.1% of the glucose

Table 1
Physiological parameters and external fluxes of aerobic and anaerobic cultures. μ is the growth rate and f is the measured conversion coefficient between OD_{600} and biomass dry weight per liter medium. Glucose (glc), acetate (ac), formate (for) and ethanol (Etoh) concentrations were measured using enzyme assay kits and O_2 and CO_2 concentrations were measured using an infrared-gas analyzer. Lactate (lac) and succinate (succ) were measured by an NMR spectroscopy (see methods). Values are given as the mean SD $n=3$. n.d.: Not detected.

	Aerobic	Anaerobic
μ (1/h)	0.58 ± 0.01	0.42 ± 0.01
f (g dry weight/od/l)	0.42 ± 0.03	0.59 ± 0.02
V_{glc} (mmol/g dry weight/h)	8.7 ± 0.5	14.9 ± 2.4
V_{O2} (mmol/g dry weight/h)	11.9 ± 1.5	0
V_{ac} (mmol/g dry weight/h)	5.8 ± 0.2	7.6 ± 0.6
V_{CO2} (mmol/g dry weight/h)	11.8 ± 1.1	n.d.
V_{Lac} (mmol/g dry weight/h)	n.d.	1.1 ± 0.1
V_{succ} (mmol/g dry weight/h)	n.d.	0.76 ± 0.09
V_{for} (mmol/g dry weight/h)	n.d.	>16.3
V_{Etoh} (mmol/g dry weight/h)	n.d.	>6.5

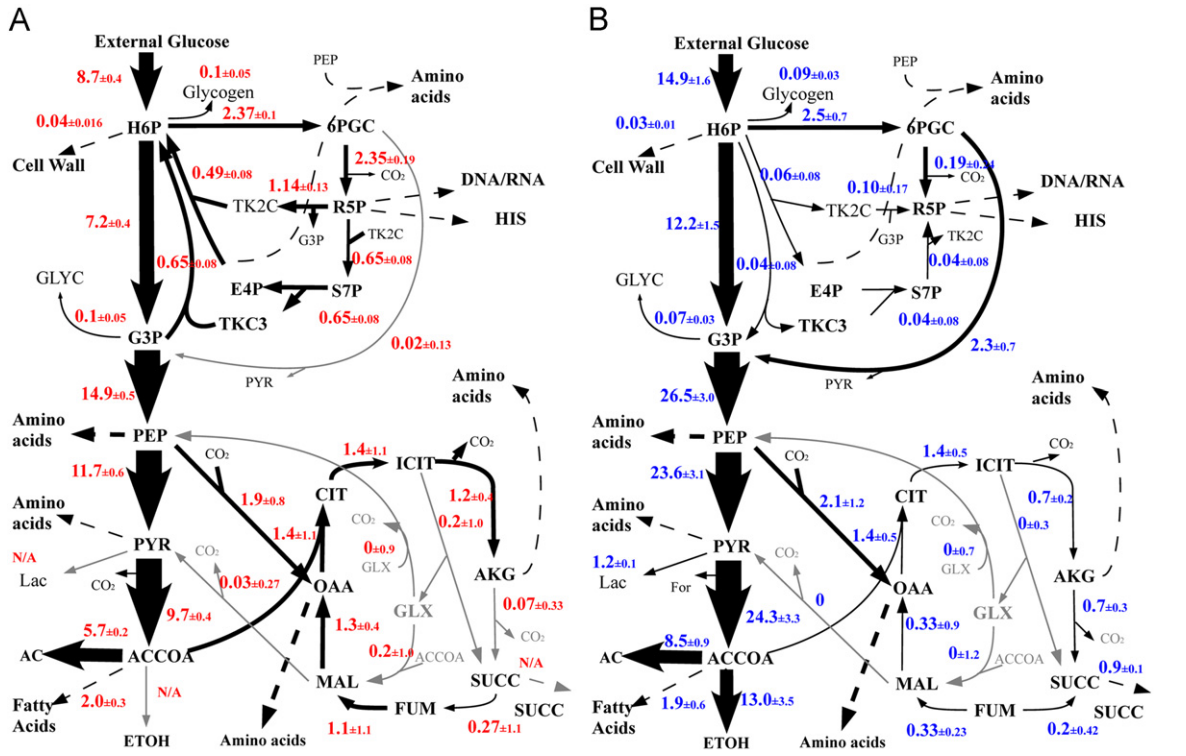

Fig. 1. ^{13}C-flux maps. ^{13}C net fluxes of central metabolism determined from best fitting with 153 (aerobic) (A) and 157 (anaerobic) (B) measurements of uptake, secretion, biomass accumulation rates and ^{13}C-labeling. Replicated cultures are $>=3$. Values represent the optimum net fluxes $\pm$ confidence intervals (see methods). All fluxes are reported as values relative to the glucose uptake rates. Reversible fluxes are listed in Table 2. Solid lines represent central metabolism reactions. Dashed lines represent non-central metabolism reactions. Gray lines represent reactions with very low activity. Size of black arrows is proportional to flux values relative to glucose uptake rates. Abbreviations: ACCOA, acetyl-coenzymeA; AC, acetate; AKG, α-ketoglutarate; CIT, citrate; ETOH, ethanol; E4P, erythrose-4-phosphate; CO_2, carbon dioxide/formate; FUM, fumarate; GLX, glyoxylate; G3P, glyceraldehyde-3-phosphate; GLYC, glycerol; HIS, histidine; H6P, hexose-6-phosphate; Lac, lactate; MAL, malate; OAA, oxaloacetate; PEP, phosphoenolpyruvate; PYR, pyruvate; R5P, pentose-phosphates; SUCC, succinate; S7P, sedoheptulose-7-phosphate; 6PGC, 6-Phospho-D-gluconate.

Table 2
Exchange fluxes of reversible reactions through metabolism.

Flux description	Aerobic flux (mmol/gDW/h)	Anaerobic flux (mmol/gDW/h)
H6P ⇔ G3P+G3P	0 ± 2.1	0 ± 5.8
E4P+TKC2P ⇔ H6P	0.5 ± 0.9	0.15 ± 0.37
R5P ⇔ G3P+TKC2P	5.4 ± 0.6	0.97 ± 2.06
Ser ⇔ Gly+mlthf	0.3 ± 0.10	0.5 ± 0.2
Thr ⇔ Accoa+Gly	0.04 ± 0.04	0.03 ± 0.17

Exchange fluxes of other reversible reactions could not be determined with the current labeling measurements. Abbreviations: ACCOA, acetyl-coenzymeA; E4P, erythrose-4-phosphate; G3P, glyceraldehyde-3-phosphate; Gly, Glycine; H6P, hexose-6-phosphate; mlthf, 5,10-methylenetetrahydrofolate; R5P, pentose-phosphates; TKC2P, the two carbon substituted enzyme intermediate in the reaction catalyzed by Transketolase; Ser, serine; Thr, threonine. Values are given as the mean $\pm$ SD $n=3$.

uptake rate. Interestingly, there is no significant flux flowing through α-ketoglutarate dehydrogenase (AKGDH) and succinyl-CoA synthetase (SUCOAS), which makes the tricarboxylic acid (TCA) cycle incomplete.

The anaerobic flux map is characterized by high flux through glycolysis, moderate flow in the OPPP, and little or no flow around the TCA cycle. The glucose uptake rate is about two fold higher in an anaerobic than an aerobic growth consistent with less efficient use of carbon for biomass production (growth). Flux going to the pentose phosphate pathway through G6PDH2r is about 16.8% of the glucose uptake rate. The TCA cycle reactions operate at low rates to produce biosynthesis precursors (α-ketoglutarate and oxaloacetate). Small amounts of fumarate are produced by nucleotide and arginine biosynthesis and most of it is reduced to succinate by succinate dehydrogenase.

3.3. *Validation of ^{13}C-metabolic flux analysis results*

In order to provide a rigorous comparison for FBA findings, and because the flux maps obtained disagree significantly with the previous reports, we performed several independent tests of the MFA results.

3.3.1. *Validation with labeling of intermediate metabolites by LC–MS*

^{13}C-labeling of intermediate metabolites which participate in glycolysis and TCA were measured to test the MFA-derived flux maps under both anaerobic and aerobic conditions (these measurements were not used in the estimation of intracellular fluxes). Labeling in intracellular glucose-6-phosphate (G6P), fructose-6-phosphate (F6P), 2/3-phosphoglycerate (3PG) and phosphoenolpyruvate (PEP) were measured using LC–MS. These additional independent labeling measurements agree well with the MFA modeling results as shown in Fig. 2, Table 3 and Fig. S7. During the construction of the ^{13}C-network, G6P and F6P are grouped into a hexose-6-phosphate pool (H6P), and 2PG, 3PG and PEP are grouped into a PEP pool (PEP). The LC–MS data also supported the grouping strategy used in ^{13}C-network construction as G6P and F6P had similar labeling patterns as did 3PG and PEP (Fig. 2).

3.3.2. *Validation of aerobic flux map using O_2 and CO_2 measurements*

CO_2 secretion and O_2 consumption rates of an aerobic culture were used to independently validate the flux map (Table 3 and Fig. 4). The measured V_{CO2} was 11.8 ± 1.1 mmol/gDW/h (Table 3)

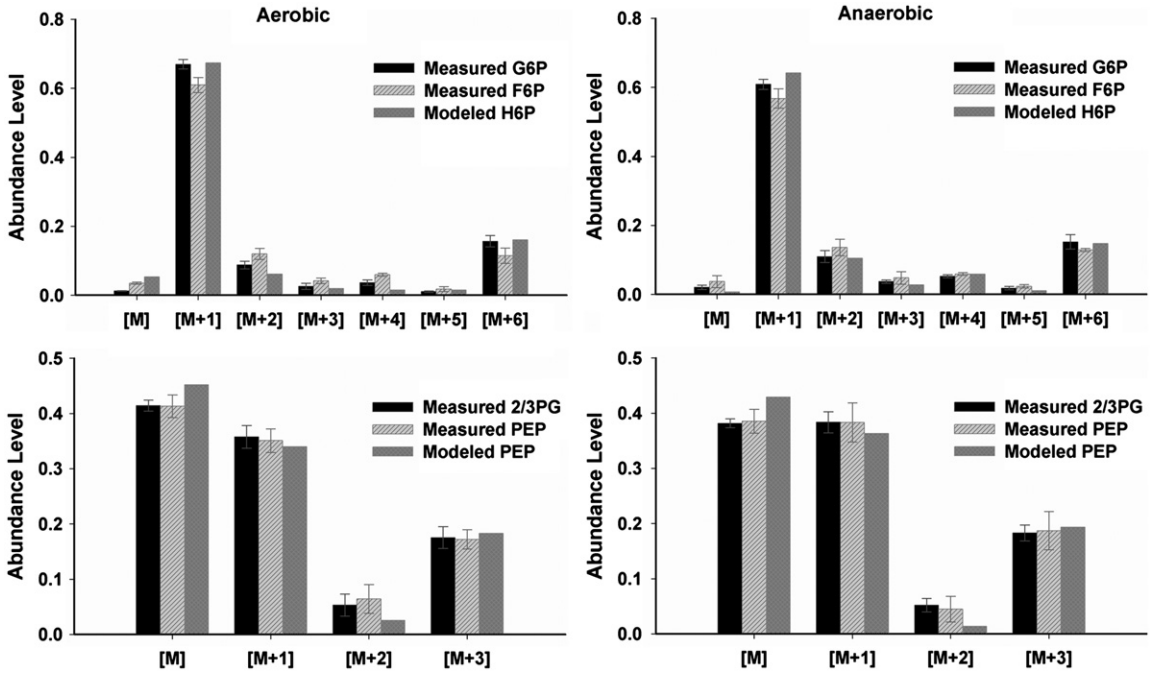

Fig. 2. Validation of flux maps using intracellular metabolite labeling measured with an LC–MS. Histograms represent the distribution of mass isomers measured and modeled for each metabolite. Error bars represent standard deviation calculated from $n \geq 2$ (G6P and F6P measurements are only 2, and the range was used in this case). 2/3PG represents the combined pool of 2-phospho-D-glycerate and 3-phospho-D-glycerate. The modeled distributions of mass isomers were calculated using flux values in Fig. 1 and Fig. S1.

Table 3
Validation of aerobic flux map by independent experiments. MFA estimations were obtained using flux values in Fig. 1 and Fig. S1 (see text).

	Validation quantity	*MFA estimation*	*Measurement or theoretical value*
Aerobic	O_2 (mmol/gDW/h)[a]	10.9 ± 0.4	11.9 ± 1.5
	CO_2 (mmol/gDW/h)	12.7 ± 0.8	11.8 ± 1.1
	Redox balance[b]	11.9 ± 0.4	11.9 ± 1.5
Anaerobic	Redox balance[b]	99.3%	100%

[a] Estimated from production and consumption of reductants in the aerobic flux map.
[b] Estimated from redox change between substrates and biomass/secreted metabolites.

and was not used in the initial MFA analysis; this measured value matched the flux estimated by an MFA (12.7 ± 0.8 mmol/gDW/h). MFA was used to estimate an O_2 consumption based on the production and consumption of reductants in the aerobic flux map (Table 3). The net production of reductant (NADH and NADPH) generated by central metabolism was obtained by summing the fluxes producing reductant and subtracting the fluxes consuming reductant in central metabolism. The amount of reductant needed to generate new biomass was calculated from the biomass production rates and reductant requirements per unit biomass component (Stephanopoulos et al., 1998). The remaining reductant was assumed to be oxidized by O_2 for ATP synthesis resulting in a calculated oxygen consumption rate (V_{O2}) of 10.9 ± 0.4 mmol/gDW/h. Uncertainty in the calculated rate of reductant production was dominated by the standard deviation of one reaction (NAD(P)H production reaction by GAPD: G3P⇔PEP). This calculated value is conservative as it does not include several minor metabolic activities which were not considered in the model and consume oxygen directly (e.g. fatty acid desaturation), but is still consistent with the measured V_{O2} (11.9 ± 1.5 mmol/gDW/h). O_2 uptake and CO_2 release are both closely connected to TCA fluxes and the agreement of these independent measurements with the flux map that strongly support the TCA flux values obtained.

3.3.3. Validation by redox balance

^{13}C isotopic MFA analysis tracks only carbon flow, but not the redox status in metabolism (Wiechert, 2001; Wittmann, 2002; Zamboni et al., 2009). The MFA solutions in the absence of labeling constraints only satisfy the balance of carbon; however, carbon-balanced solutions are not necessarily balanced in redox. Since the balances of redox states between feeding substrates and the biomass and secreted metabolites were not used in the MFA analysis (which is based only on labeling and measured external fluxes), and they provide another independent way to validate the MFA predictions. The redox balance was considered for both aerobic and anaerobic conditions (Table 3). In the aerobic case, the secreted products and accumulated biomass create a change of the redox state that can be offset by an electron transport. As an electron transport is dependent on oxygen consumption, measuring the uptake of oxygen and comparing with that of the model provide a check of the model assumptions and results. Under anaerobic conditions, the redox state of substrates must match what is produced in biomass and products, because there is no O_2 present (Allen et al., 2009). Comparison between experimental and modeled numbers shows agreement in both cases. Aerobic cultures consume 11.9 ± 1.5 mmol/gDW/h O_2 consistent with the model-determined value of 11.9 ± 0.4 mmol/gDW/h. Here again the standard deviation was dominated by the uncertainty in the NAD(P)H production reaction rate GAPD: G3P⇔PEP. In the anaerobic case, a redox change of 0.04 in biomass per glucose uptake was obtained, representing 99% or greater agreement between substrate uptake rates, biomass composition and secretion rates for the redox state of carbon.

3.4. ATP maintenance costs in aerobic and anaerobic culture

Fig. 3 compares ATP production and consumption for biomass production and maintenance under aerobic and anaerobic

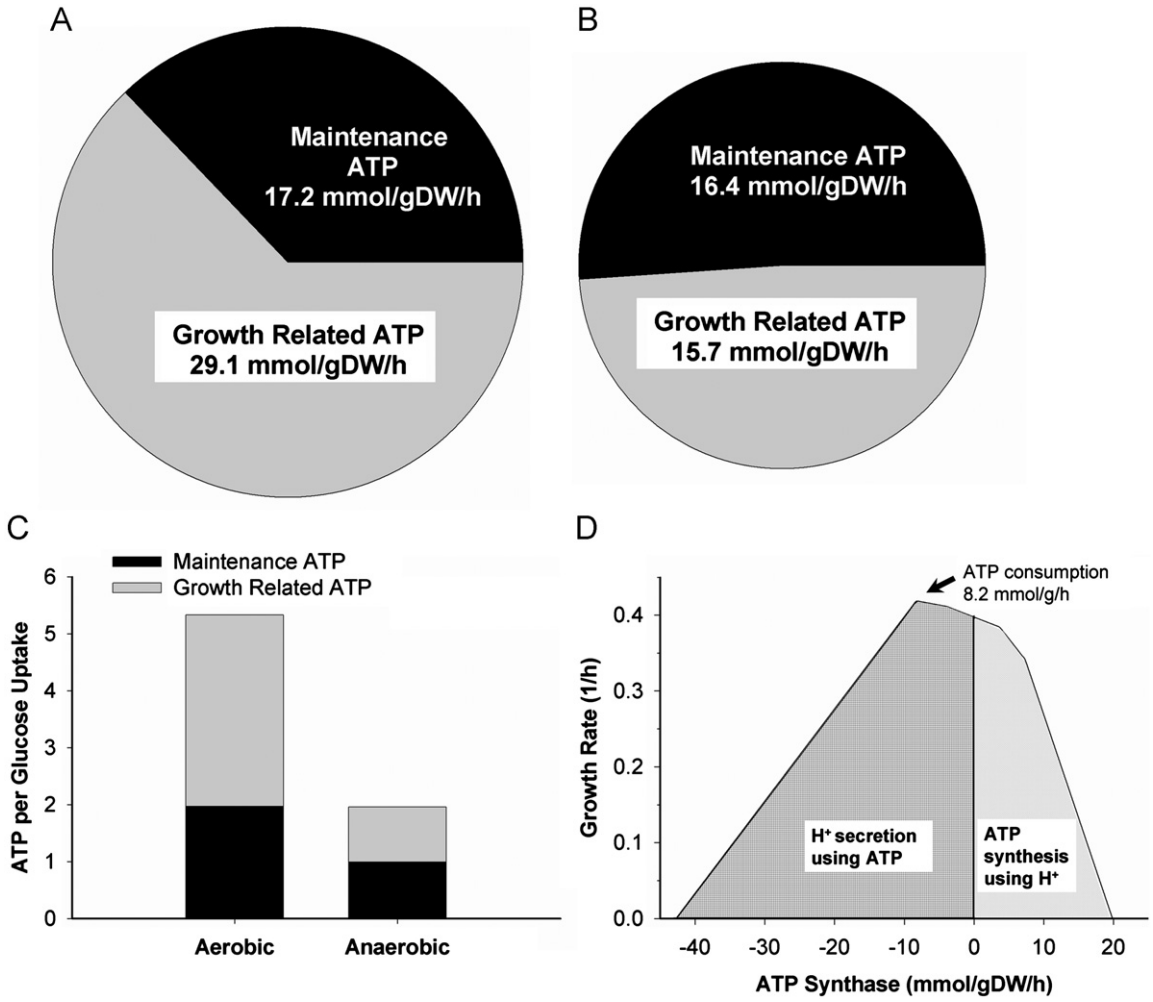

Fig. 3. ATP production and utilization in aerobic and anaerobic metabolisms. ATP production and utilization rates in units of mmol/gDW/h are shown for the aerobic (A) and anaerobic conditions (B). ATP production and utilization rates per glucose uptake rate are shown in (C). An FBA predicted activity of anaerobic ATP synthase, using the robustness analysis (D). ATP synthase catalyzes the reaction: $ADP_{[c]}+Pi_{[c]}+4H^{+}_{[c]}=ATP_{[c]}+H_2O_{[c]}+3H^{+}_{[m]}$, where subscript c and m represent cytoplasm and inter-membrane space. Glucose and O_2 uptake rates of 16.8 and 0 mmol/gDW/h were supplied to the FBA model to simulate the anaerobic culture with growth rate of 0.42 1/h. ATP synthase consumes 8.2 mmol/gDW/h ATP during maximal growth state.

conditions. We define the ATP maintenance cost to be the difference between the rate of ATP synthesized metabolically and the ATP consumed in the biomass production. For an aerobic growth, surplus reductant was converted to an ATP using the P/O ratios previously described (Feist et al., 2007). The maintenance was calculated to consume 17.2 mmol ATP/gDW/h. For the anaerobic culture, the reductant was nearly balanced and made no significant contribution to the ATP production, which is predominantly glycolytic. The resulting ATP maintenance flux was 16.4 mmol/gDW/h. Aerobic culture produces about 5.3 ATP per glucose consumed (or 46.3 mmol ATP/gDW/h) via central metabolism and respiration, and ATP maintenance accounts for 37.2% of the production. Anaerobic cultures produce about 1.96 ATP per glucose uptake (or 32.1 mmol ATP/gDW/h) via central metabolism, and about 51.1% is used for maintenance.

3.5. Flux balance analysis

FBA was used to predict the cellular growth rate in aerobic and anaerobic cultures. Aerobic growth rates were first predicted using only the measured glucose uptake rate, and then FBA predictions were made by further constraining both the measured glucose and O_2 uptake rates and maximizing growth rate (referred to as O_2-limited predictions). The O_2-limited prediction of growth rate (0.65 ± 0.08 1/h) is consistent with the observed growth rates in both regular aerobic and O_2-enhanced culture (0.58 ± 0.08 1/h). The predicted growth rate without the O_2 uptake constraint (0.80 ± 0.05 1/h) is significantly higher (38%) than the measured growth rate. The anaerobic growth rate (0.38 ± 0.08 1/h) was also predicted by an FBA using the measured glucose uptake rate and with a zero O_2 uptake rate, and is consistent with the measured growth rate (0.42 ± 0.01 1/h). Standard deviations in the FBA prediction were obtained from the measurement standard deviations on the glucose and O_2 uptake rates.

FBA was used to predict the secretion rates of metabolites and internal fluxes. The FBA predicted product secretion rates that agree well with MFA results (Fig. S2 in Supplemental materials), even though these were not used as constraints in the prediction. The range of the internal fluxes corresponding to measured growth rates were obtained by Flux Variability Analysis (FVA) (Becker et al., 2007). As shown in Fig. 5A, an FBA predicts a fairly wide range of flux values for the OPPP reactions (0–32% of glucose uptake rate at G6PDH2r). The sampling results show that most flux distributions of the OPPP are close to zero, and substantially lower than MFA-derived fluxes (Fig. 5B). For example, the flux through G6PDH2r yielded from sampling is between 0 and 1 mmol/gDW/h, while the experimentally derived flux from an MFA is 2.5 ± 0.7 mmol/gDW/h.

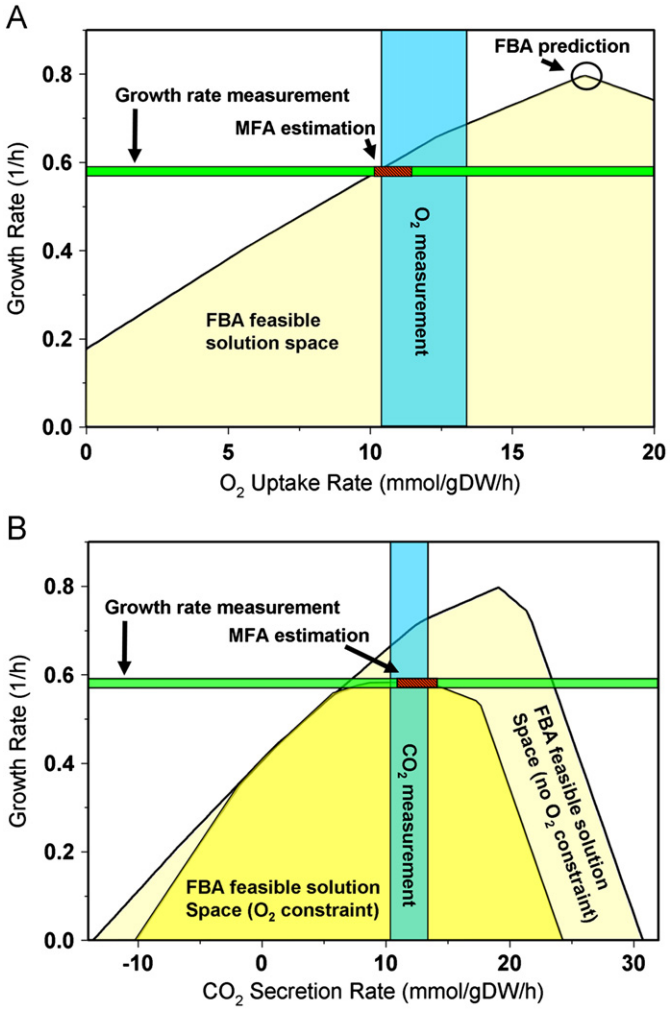

Fig. 4. Aerobic O_2 consumption rate (A) and CO_2 secretion rate (B) determined by an FBA robustness analysis, MFA and direct measurements. Glucose uptake rate (8.7 mmol/gDW/h) was used for an FBA prediction in both A and B. An O_2 uptake rate of 10.4 mmol/gDW/h was used in O_2 constraint FBA prediction to simulate the observed aerobic growth (μ=0.58 1/h). Unlimited O_2 supply was assumed for no-O_2-constraint FBA prediction.

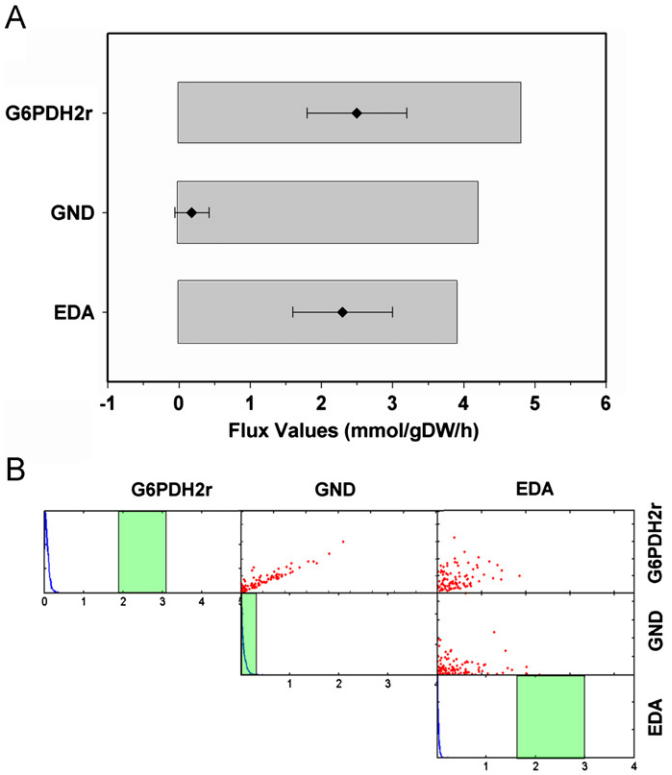

Fig. 5. Comparison of anaerobic internal fluxes from MFA and FBA. Glucose and O_2 uptake rates of 16.8 and 0 mmol/gDW/h were used to constrain the FBA model to simulate the anaerobic culture with measured growth rate (0.42 1/h). The growth rate in the FBA model was constrained between 95% and 100% of the measured value. (A) Ranges of pentose phosphate pathway fluxes predicted from Flux Variability Analysis. Triangles represent an MFA estimation. (B) FBA predicted flux distribution by uniform random sampling of metabolic solution space, using the Cobra toolbox (see methods). Green bars represent values obtained from an MFA. Abbreviations: G6PDH2r, glucose-6-phosphate dehydrogenase; GND, phosphogluconate dehydrogenase; EDA, 2 dehydro 3 deoxy phosphogluconate aldolase.

We also used the constraint-based model to examine the sensitivity of the maximal growth rate to an ATP synthase activity using the robustness analysis (Fig. 3D) (Mahadevan and Schilling, 2003). Glucose and O_2 uptake rates of 16.8 and 0 mmol/g/h were constrained in the model to simulate the anaerobic culture. ATP synthase was predicted to operate in reverse, consuming an ATP to expel protons to maintain the intracellular pH and consumes about 8.2 mmol/g/h ATP at the observed growth rate of 0.42 1/h.

4. Discussion

4.1. TCA, Glycolytic and OPPP fluxes

The aerobic flux map revealed moderate carbon flux entering the non-cyclic TCA reactions (16.1% of glucose uptake rate). The moderate flux through CS and ACONT is consistent with previous ^{13}C-labeling flux analyses (Nicolas et al., 2007) and (Fischer and Sauer, 2003), but these studies reported a complete TCA cycle, which disagrees with the results obtained here.

To further test the TCA flux values, we had made measurements of labeling in intracellular CO_2/HCO_3^- based on labeling in the terminal carbon of arginine, which is made directly from CO_2/HCO_3^-. The GC–MS based CO_2 labeling values (see Table S6) of 31 $\pm$ 0.02% agrees well with model predicted CO_2 labeling (32%). This additional measurement therefore supports our flux map predicted TCA activity. We also used FBA to predict the aerobic growth rate by constraining the AKGDH and SUCOAS fluxes to zero. Glucose and O_2 uptake rates were set to be the same as in Fig. 2A. The results also show that zero fluxes of AKG and SUCOAS do not alter the predicted maximal growth rates in Fig. 2A. This finding seems surprising since AKGDH and SUCOAS produce two NADH (which aerobically can be converted into ATP) and two ATP. The lack of cyclic operation of TCA cycle may reflect the reduced availability of the electron transport chain for NADH recycling in these cells (as discussed below in the context of oxygen use). The biosynthesis flux maps reveal a significant production of fumarate (9.4% of glucose uptake rate) as a by-product from RNA/DNA and arginine synthesis (Fig. S1 in Supplemental materials) which are substantial, but appear not to have been included in most previous MFA analyses (Emmerling et al., 2002; Fischer and Sauer, 2003; Fischer et al., 2004; Nicolas et al., 2007; Peng et al., 2004; Schmidt et al., 1999; Zhao and Shimizu, 2003). However, differences in the exact growth conditions and/or differences between wildtype strains in some of these studies may also contribute to the different TCA fluxes in this study and prior studies. Studies that included fumarate production from RNA/DNA and arginine synthesis involved very different strains (Antoniewicz et al., 2007b) or species (Masakapalli et al., 2010).

The anaerobic flux map showed high fluxes through glycolysis (81.9% of glucose uptake at glucose-6-phophate isomerase) and moderate fluxes through the OPPP (16.8% of glucose uptake). We calculated the net production of redox carriers in central metabolism, and found that the OPPP is secondary to glycolysis as a source of reductant. Schmidt et al. (1999) examined fermentation in *E. coli* W3110 by an MFA using an NMR labeling data (Szyperski, 1995) and by-product secretion rates (Ingraham et al., 1995) from the literature, and reported very high fluxes(74% of glucose uptake) through glucose-6-phosphate dehydrogenase (G6PDH2r) for an anaerobic growth (Schmidt et al., 1999). The difference between OPPP fluxes measured here and the values reported by Schmidt et al. (1999)may be caused in part by the use of a different strain from the one used here and/or by their use of literature values for the by-product secretion rates that were obtained in experiments with strains and growth rates different from those used in the labeling experiments.

4.2. Regulation of metabolic efficiency by proton transport across membrane

Cells require energy for maintenance in addition to growth (defined as net biomass production). Maintenance activity includes transport of substrate and product metabolites and ions for homeostasis, as well as turnover of cell components. The maintenance energy for aerobic and anaerobic growths was found to be 17.2 and 16.4 mmol ATP/gDW/h, respectively, accounting for 37.2% and 51.1% of the total ATP produced. The maintenance ATP per unit biomass production was calculated to be 29.7 mmol/gDW for an aerobic growth and 39.1 mmol/gDW for anaerobic growth. The one third increase in anaerobic maintenance energy per gram production of biomass obtained here indicates a striking change of intracellular maintenance activity.

The energetic cost of secreting protons produced in fermentative metabolism may contribute to a significant portion of an increased ATP maintenance observed during anaerobic growth. The FBA predicted growth rate of anaerobically cultured *E. coli* assuming an ATP maintenance flux of 7.6 mmol ATP/gDW/h (Reed et al., 2003) was 0.38 ± 0.08, which is in agreement with our measurement of 0.42 ± 0.01. The results of this FBA analysis were examined for all reactions that consume ATP at the maximal growth rates, which identified ATP synthase as the main consumer of ATP in addition to the growth reaction.

We used robustness analysis (Mahadevan and Schilling, 2003) to test the sensitivity of maximal growth rate to flux through ATP synthase (Fig. 3D) (Becker et al., 2007). ATP synthase is required to consume about 8.3 mmol/gDW/h of ATP in order to maintain the maximal growth rate of the cells. The ATP was assumed to pump four protons per ATP (Reed et al., 2003) from the cytoplasm across the cell membrane. Thus, the increased maintenance ATP in anaerobic growth is not due to more membrane leakage or higher costs of substrate uptake than an aerobic growth, as has been suggested (Stouthamer and Bettenhaussen, 1977). It is due to the need to secrete excess protons accumulated during fermentation to maintain an intracellular pH. The electron transfer chain does not function in an anaerobic growth; therefore, the secretion of protons must be achieved via ATP synthase. This maintenance ATP thus appears to decrease the metabolic efficiency of *E. coli* under anaerobic conditions.

To test the idea of intracellular proton accumulation reducing ATP availability for growth, we created an in-silico 'knock-in' strain from the wildtype iJR904 FBA model. The 'knock-in' strain allowed Formate Hydrogen Lyase (FDH) activity by introducing two reactions into iJR904 allowing for the removal of hydrogen (a product of FDH): hydrogen diffusion through the cytoplasm to the cell membrane and hydrogen diffusion across the membrane to the media. The product secretion and growth rates were predicted for the 'knock-in' strain and the wild-type (Table S3 in Supplementary materials). Maximal growth was still assumed as the objective function for this anaerobic prediction, and the same glucose uptake rate of 16.8 mmol/gDW/h was used in both cases. Similar secretion rates were predicted in both the 'knock-in' and wildtype for most end-products, except that the formate production was replaced by CO_2. But a 16% increase in the growth rate and a yield of H_2 (28.0 mmol/gDW/h) are predicted in addition to the ethanol production (13.0 mmol/gDW/h). H_2 is a clean bioenergy substitutes for fossil fuels. Therefore, knocking in formate hydrogen lyase to ethanol producing E coli yields a biofuel by-product at no added cost. Yoshida et al. (2005) constructed FHL overexpressing *E coli.* strains for hydrogen production. The mutants were constructed in *E. coli* W3110 by inactivating the FHL repressor (*hycA*) alone (SR12) and in combination with overexpressing the FHL activator (*fhlA*) (SR13). The cells were cultured anaerobically in the BC medium with 100 mM glucose. In addition to H_2 production, the mutant showed a 25% higher growth rate under anaerobic conditions in the BC medium supplied with glucose. These observations are consistent with our prediction that over-expressing FHL in an anaerobic grown *E. coli* may reduce intracellular proton accumulation, saving ATP for biomass production and producing H_2 at the same cost. Therefore, reduction of ATP expenditure on proton secretion may have practical potential in fermentative bioenergy production.

4.3. Limited oxidative phosphorylation results in submaximal aerobic growth

FBA and MFA can be used to test the metabolic optimality of organisms under the designed selective pressure. It has been assumed in most FBA studies that cells maximize growth under glucose limited conditions (Ibarra et al., 2002; Pramanik and Keasling, 1998; Reed and Palsson, 2004). We measured the growth rate of aerobically cultured *E. coli*, and found it to be 30% less than the rate predicted by FBA if the glucose uptake rate is the only limiting factor for cell growth. The aerobic MFA flux map also showed that the CS and ACONT fluxes are $< 20\%$ of the glucose uptake rate, indicating potentially non-optimal ATP production. On the other hand, the growth is predicted by an FBA to be close to the observed rate if both glucose and oxygen uptake fluxes are constrained to be at their experimentally measured values.

These results suggest that the maximal growth of the cell is repressed either by the availability of environmental O_2 or by the ability to move electrons through the electron transfer chain. We examined the effect of elevated O_2 (35% O_2 level in the headspace), but found no change in growth rate compared to normoxic conditions (Fig. S3 in Supplemental materials). Therefore, O_2 availability seems not to be limiting, and thus repressed oxidative phosphorylation may be responsible for the non-maximal growth. Decreased rates through oxidative phosphorylation would restrict the consumption rate of reductant (NADH and FADH2), resulting in the modest TCA cycle fluxes seen in the aerobic flux map. This is in agreement with the hypothesis based on a thermodynamics analysis by Heijnen (1991, 2009, 1999) that the capacity of the electron transport chain is a key factor limiting cell growth, Our result is also consistent with the transcriptional analysis of wild-type *E. coli* and a mutant overexpressing NADH oxidase (Vemuri et al., 2006). As glucose uptake rate was increased, some of the genes involved in TCA cycle and respiration were repressed in wild-type cells. This repression was relieved in cells over-expressing an NADH oxidase.

This raises the question of why selective pressure fails to result in the maximal growth efficiency. One possible explanation is that

the wild-type MG1655 *E. coli* strain is not optimized for growth under these conditions. Adaptive evolution of *E. coli* MG1655 on glucose in minimal media over 500 generations, led to increased growth rates as well as glucose and O_2 uptake rates (Ibarra et al., 2002). However, these evolved strains do not show consistent significant changes in the glucose to oxygen uptake ratio, suggesting no relative increase in the expression of respiratory chain proteins to glucose uptake proteins. Further work is required to determine whether additional constraints are responsible for the apparent suboptimal growth rate or whether a longer term adaptive evolution would lead to an improved growth efficiency of *E. coli* under limited glucose supply.

4.4. Prediction of external and internal fluxes by FBA

FBA is successful in predicting external fluxes (net entry into and efflux from the metabolic network) given sufficient knowledge of the network and enough measurements to constrain the feasible range of flux patterns. Maximal growth is generally used as the objective function in FBA (Pramanik and Keasling, 1998; Varma and Palsson, 1993). However, biological systems may function with different (Schuetz et al., 2007) or multiple objectives and constraining the solution space with more measurements may be needed to bypass the requirement for these unknown objectives or physicochemical constraints in FBA. Thus, we have shown above that *E. coli* does not grow at the predicted maximal rates in an aerobic batch culture in glucose minimal media and that further constraining the constraint-based model's solution space with oxygen uptake rate measurements improved the FBA predictions for growth rate and by-product secretion rates. Since O_2 availability is not limiting (based on our O_2-enhanced experiments and estimates of O_2 concentrations), this implies that the activities of respiratory enzymes are insufficient for efficient degradation of glucose due to unknown but potentially, biologically important reasons.

FBA has a limited ability to predict internal fluxes. While the fluxes established from an MFA were within the FBA feasible range, the values of MFA-derived fluxes differ substantially from the most-frequently predicted values of internal fluxes yielded from sampling the feasible space. This implies that a number of flux distributions may be shared by silent phenotypes, but are not necessarily useful in describing the actual distribution of internal fluxes. Therefore, caution should be exercised when interpreting internal flux distributions obtained by choosing an arbitrary set of results from FBA linear programming solvers or by randomly or systematically sampling the solution space in the absence of an experimentally derived MFA flux map.

5. Conclusion

MFA describes the metabolic status of a biological system by determining its intracellular carbon flow. A genome-scale constraint-based model contains the full stoichiometric description of a biological system and predicts the metabolic capacities of the system, using the pre-assumed objectives. Comparing the theoretical capacities with the working status can bring new physiological discoveries. For example, in this study, we showed from the synergy of MFA and FBA that TCA is non-cyclic in an aerobic growth of *E. coli* on glucose in defined media and that the suboptimal growth is due to the limited oxidative phosphorylation. In addition, FBA is able to pinpoint key reactions that restrict an MFA established metabolic network from reaching its full metabolic capacities, and thus provides directions for rational strain design. It was possible here to identify a potential target, formate hydrogen lyase, for improving the biofuel application. Therefore, both rational strain design and physiological insight from metabolic flux analysis benefit substantially from the use of both FBA and MFA, using the same underlying network and experimental conditions.

Acknowledgments

The authors would like to thank Dr. Daniel Holmes (MSU Max T Rogers NMR Facility), Mrs. Beverly Chamberlin (MSU Mass Spectrometry Facility) and Dr. Randy Beaudry (Postharvest Biology and Technology Lab, MSU, IRGA/L2 paramagnetic analysis) for an expert help with instrumental analyses. We are also grateful to Dr. Hart Poskar for writing software (ClusterFLUX) used in MFA computations, and *Inga* Krassovskaya, Dr. Chunjie Tian, Dr. Igor Libourel and Dr. Rahul Deshpande for valuable discussions. This work was supported by the DOE Great Lakes Bioenergy Research Center and by the Michigan State University.

Appendix A. Supporting information

Supplementary data associated with this article can be found in the online version at doi:10.1016/j.ymben.2010.11.004.

References

Allen, D.K., Ohlrogge, J.B., Shachar-Hill, Y., 2009. The role of light in soybean seed filling metabolism. Plant J. 58, 220–234.

Allen, D.K., Shachar-Hill, Y., Ohlrogge, J.B., 2007. Compartment-specific labeling information in ^{13}C metabolic flux analysis of plants. Phytochemistry 68, 2197–2210.

Alonso, A.P., Piasecki, R., Yan, W., LaClair, R., Shachar-Hill, Y., 2010. Quantifying levels and labeling of plant cell wall precursors using ion chromatography tandem mass spectrometry. Plant Physiology. Under Review.

Antoniewicz, M.R., Kelleher, J.K., Stephanopoulos, G., 2007a. Elementary metabolite units (EMU): a novel framework for modeling isotopic distributions. Metab. Eng. 9, 68–86.

Antoniewicz, M.R., Kraynie, D.F., Laffend, L.A., Gonzalez-Lergier, J., Kelleher, J.K., Stephanopoulos, G., 2007b. Metabolic flux analysis in a nonstationary system: fed-batch fermentation of a high yielding strain of *E. coli* producing 1,3-propanediol. Metab. Eng. 9, 277–292.

Becker, S.A., Feist, A.M., Mo, M.L., Hannum, G., Palsson, B.O., Herrgard, M.J., 2007. Quantitative prediction of cellular metabolism with constraint-based models: the COBRA Toolbox. Nat. Protocols 2, 727–738.

Boghigian, B.A., Seth, G., Kiss, R., Pfeifer, B.A., 2010. Metabolic flux analysis and pharmaceutical production. Metab. Eng. 12, 81–95.

Bolten, C.J., Kiefer, P., Letisse, F., Portais, J.C., Wittmann, C., 2007. Sampling for metabolome analysis of microorganisms. Anal. Chem. 79, 3843–3849.

Bordel, S., Nielsen, J., 2010. Identification of flux control in metabolic networks using non-equilibrium thermodynamics. Metab. Eng. 12, 369–377.

Dieuaide-Noubhani, M., Raffard, G., Canioni, P., Pradet, A., Raymond, P., 1995. Quantification of compartmented metabolic fluxes in maize root tips using isotope distribution from ^{13}C- or ^{14}C-labeled glucose. J. Biol. Chem. 270, 13147–13159.

Edwards, J.S., Palsson, B.O., 2000. Robustness analysis of the *Escherichia coli* metabolic network. Biotechnol. Prog. 16, 927–939.

Emmerling, M., Dauner, M., Ponti, A., Fiaux, J., Hochuli, M., Szyperski, T., Wuthrich, K., Bailey, J.E., Sauer, U., 2002. Metabolic flux responses to pyruvate kinase knockout in Escherichia coli. J. Bacteriol. 184, 152–164.

Feist, A.M., Henry, C.S., Reed, J.L., Krummenacker, M., Joyce, A.R., Karp, P.D., Broadbelt, L.J., Hatzimanikatis, V., Palsson, B.O., 2007. A genome-scale metabolic reconstruction for *Escherichia coli* K-12 MG1655 that accounts for 1260 ORFs and thermodynamic information. Mol. Syst. Biol. 3, 121.

Feist, A.M., Herrgard, M.J., Thiele, I., Reed, J.L., Palsson, B.O., 2009. Reconstruction of biochemical networks in microorganisms. Nat. Rev. Microbiol. 7, 129–143.

Fischer, E., Sauer, U., 2003. A novel metabolic cycle catalyzes glucose oxidation and anaplerosis in hungry *Escherichia coli*. J. Biol. Chem. 278, 46446–46451.

Fischer, E., Zamboni, N., Sauer, U., 2004. High-throughput metabolic flux analysis based on gas chromatography-mass spectrometry derived ^{13}C constraints. Anal. Biochem. 325, 308–316.

Fong, S.S., Burgard, A.P., Herring, C.D., Knight, E.M., Blattner, F.R., Maranas, C.D., Palsson, B.O., 2005. In silico design and adaptive evolution of *Escherichia coli* for production of lactic acid. Biotechnol. Bioeng. 91, 643–648.

Goffman, F.D., Alonso, A.P., Schwender, J., Shachar-Hill, Y., Ohlrogge, J.B., 2005. Light enables a very high efficiency of carbon storage in developing embryos of rapeseed. Plant Physiol. 138, 2269–2279.

Heijnen, J.J., 1991. A new thermodynamically based correlation of chemotrophic biomass yields. Antonie Van Leeuwenhoek. 60, 235–256.
Heijnen, J.J., 2009. Thermodynamic description of microbial growth and product formation. In: Smolke, C.D. (Ed.), The Metabolic Pathway Engineering Handbook: Fundamentals. CRC Press, Boca Raton, FL.
Heijnen, S., 1999. Bioenergetics of microbial growth. In: Flickinger, M.C., Drew, S.W. (Eds.), Encyclopedia of Bioprocess technology, Fermentation, Biocatalysis and Bioseparation. John Wiley and Sons, New York.
Hua, Q., Joyce, A.R., Fong, S.S., Palsson, B.O., 2006. Metabolic analysis of adaptive evolution for in silico-designed lactate-producing strains. Biotechnol. Bioeng. 95, 992–1002.
Hua, Q., Yang, C., Baba, T., Mori, H., Shimizu, K., 2003. Responses of the central metabolism in *Escherichia coli* to phosphoglucose isomerase and glucose-6-phosphate dehydrogenase knockouts. J. Bacteriol. 185, 7053–7067.
Ibarra, R.U., Edwards, J.S., Palsson, B.O., 2002. *Escherichia coli* K-12 undergoes adaptive evolution to achieve in silico predicted optimal growth. Nature 420, 186–189.
Ingraham, J.L., Maaloe, O., Neidhardt, F.C., 1995. Growth of the Bacterial Cell. Sinauer Associates, Sunderland, MA.
Jiao, Z., Baba, T., Mori, H., Shimizu, K., 2003. Analysis of metabolic and physiological responses to gnd knockout in *Escherichia coli* by using C-13 tracer experiment and enzyme activity measurement. FEMS Microbiol. Lett. 220, 295–301.
Khannapho, C., Zhao, H., Bonde, B.K., Kierzek, A.M., Avignone-Rossa, C.A., Bushell, M.E., 2008. Selection of objective function in genome scale flux balance analysis for process feed development in antibiotic production. Metab. Eng. 10, 227–233.
Kim, H.U., Kim, T.Y., Lee, S.Y., 2008. Metabolic flux analysis and metabolic engineering of microorganisms. Mol. Biosyst. 4, 113–120.
Kim, S., Seol, E., Oh, Y.-K., Wang, G.Y., Park, S., 2009. Hydrogen production and metabolic flux analysis of metabolically engineered *Escherichia coli* strains. Int. J. Hydrogen Energy 34, 7417–7427.
Koffas, M., Stephanopoulos, G., 2005. Strain improvement by metabolic engineering: lysine production as a case study for systems biology. Curr. Opinion Biotechnol. 16, 361–366.
Lee, K., Berthiaume, F., Stephanopoulos, G.N., Yarmush, M.L., 1999. Metabolic flux analysis: a powerful tool for monitoring tissue function. Tissue Eng. 5, 347–368.
Liao, J.C., Oh, M.K., 1999. Toward predicting metabolic fluxes in metabolically engineered strains. Metab. Eng. 1, 214–223.
Lin, Y., Tanaka, S., 2006. Ethanol fermentation from biomass resources: current state and prospects. Appl. Microbiol. Biotechnol. 69, 627–642.
Mahadevan, R., Schilling, C.H., 2003. The effects of alternate optimal solutions in constraint-based genome-scale metabolic models. Metab. Eng. 5, 264–276.
Masakapalli, S.K., Le Lay, P., Huddleston, J.E., Pollock, N.L., Kruger, N.J., Ratcliffe, R.G., 2010. Subcellular flux analysis of central metabolism in a heterotrophic Arabidopsis cell suspension using steady-state stable isotope labeling. Plant Physiol. 152, 602–619.
Meadows, A.L., Karnik, R., Lam, H., Forestell, S., Snedecor, B., 2010. Application of dynamic flux balance analysis to an industrial *Escherichia coli* fermentation. Metab. Eng. 12, 150–160.
Nanchen, A., Fuhrer, T., Sauer, U., 2007. Determination of metabolic flux ratios from ^{13}C-experiments and gas chromatography-mass spectrometry data: protocol and principles. Methods Mol. Biol. 358, 177–197.
Neidhardt, F.C., 1996. *Escherichia Coli* and *Salmonella*: Cellular and Molecular Biology. American Society for Microbiology.
Neidhardt, F.C., Edwin Umbarger, H., 1996. Chemical composition of *Escherichia coli*. In: Neidhardt, F.C. (Ed.), *Escherichia coli* and *Salmonella*: Cellular and Molecular Biology. American Society for Microbiology, Washington, D.C.
Nicolas, C., Kiefer, P., Letisse, F., Kromer, J., Massou, S., Soucaille, P., Wittmann, C., Lindley, N.D., Portais, J.C., 2007. Response of the central metabolism of *Escherichia coli* to modified expression of the gene encoding the glucose-6-phosphate dehydrogenase. FEBS Lett. 581, 3771–3776.
Papp, B., Pal, C., Hurst, L.D., 2004. Metabolic network analysis of the causes and evolution of enzyme dispensability in yeast. Nature 429, 661–664.
Park, J.H., Lee, K.H., Kim, T.Y., Lee, S.Y., 2007. Metabolic engineering of *Escherichia coli* for the production of L-valine based on transcriptome analysis and in silico gene knockout simulation. In: Proc. Natl. Acad. Sci. USA 104, 7797–7802.
Peng, L., Arauzo-Bravo, M.J., Shimizu, K., 2004. Metabolic flux analysis for a ppc mutant *Escherichia coli* based on ^{13}C-labelling experiments together with enzyme activity assays and intracellular metabolite measurements. FEMS Microbiol. Lett. 235, 17–23.
Pramanik, J., Keasling, J.D., 1998. Effect of *Escherichia coli* biomass composition on central metabolic fluxes predicted by a stoichiometric model. Biotechnol. Bioeng. 60, 230–238.
Price, N.D., Reed, J.L., Palsson, B.O., 2004. Genome-scale models of microbial cells: evaluating the consequences of constraints. Nat. Rev. Microbiol. 2, 886–897.
Ratcliffe, R.G., Shachar-Hill, Y., 2006. Measuring multiple fluxes through plant metabolic networks. Plant J. 45, 490–511.
Reed, J.L., Palsson, B.O., 2004. Genome-scale in silico models of E-coli have multiple equivalent phenotypic states: assessment of correlated reaction subsets that comprise network states. Genome Res. 14, 1797–1805.
Reed, J.L., Vo, T.D., Schilling, C.H., Palsson, B.O., 2003. An expanded genome-scale model of *Escherichia coli* K-12 (iJR904 GSM/GPR). Genome Biol. 4, R54.
Rontein, D., Dieuaide-Noubhani, M., Dufourc, E.J., Raymond, P., Rolin, D., 2002. The metabolic architecture of plant cells. Stability of central metabolism and flexibility of anabolic pathways during the growth cycle of tomato cells. J. Biol. Chem. 277, 43948–43960.
Sambrook, J., Russel, D.W., 2001. Molecular Cloning, A Laboratory Manual. Cold Spring Harbor Laboratory Press, Cold Spring Habor, NY.
Sauer, U., 2006. Metabolic networks in motion: ^{13}C-based flux analysis. Mol. Syst. Biol. 2, 62.
Sauer, U., Lasko, D.R., Fiaux, J., Hochuli, M., Glaser, R., Szyperski, T., Wuthrich, K., Bailey, J.E., 1999. Metabolic flux ratio analysis of genetic and environmental modulations of *Escherichia coli* central carbon metabolism. J. Bacteriol. 181, 6679–6688.
Schmidt, K., Carlsen, M., Nielsen, J., Villadsen, J., 1997. Modeling isotopomer distributions in biochemical networks using isotopomer mapping matrices. Biotechnol. Bioeng. 55, 831–840.
Schmidt, K., Nielsen, J., Villadsen, J., 1999. Quantitative analysis of metabolic fluxes in *Escherichia coli*, using two-dimensional NMR spectroscopy and complete isotopomer models. J. Biotechnol. 71, 175–189.
Schuetz, R., Kuepfer, L., Sauer, U., 2007. Systematic evaluation of objective functions for predicting intracellular fluxes in *Escherichia coli*. Mol. Syst. Biol. 3, 119.
Schwender, J., Ohlrogge, J.B., Shachar-Hill, Y., 2003. A flux model of glycolysis and the oxidative pentosephosphate pathway in developing *Brassica napus* embryos. J. Biol. Chem. 278, 29442–29453.
Segre, D., Vitkup, D., Church, G.M., 2002. Analysis of optimality in natural and perturbed metabolic networks. Proc. Natl. Acad. Sci. USA 99, 15112–15117.
Shlomi, T., Berkman, O., Ruppin, E., 2005. Regulatory on/off minimization of metabolic flux changes after genetic perturbations. Proc. Natl. Acad. Sci. USA 102, 7695–7700.
Stephanopoulos, G., 1999. Metabolic fluxes and metabolic engineering. Metab. Eng. 1, 1–11.
Stephanopoulos, G.N., Aristidou, A.A., Nielsen, J., 1998. Metabolic Engineering—Principles and Methodologies. Academic Press, San Diego.
Stouthamer, A.H., Bettenhaussen, C.W., 1977. A continuous culture study of an ATPase-negative mutant of *Escherichia coli*. Arch. Microbiol. 113, 185–189.
Suthers, P.F., Chang, Y.J., Maranas, C.D., 2010. Improved computational performance of MFA using elementary metabolite units and flux coupling. Metab. Eng. 12, 123–128.
Szyperski, T., 1995. Biosynthetically directed fractional ^{13}C-labeling of proteinogenic amino acids. An efficient analytical tool to investigate intermediary metabolism. Eur. J. Biochem. 232, 433–448.
Tang, Y.J., Martin, H.G., Myers, S., Rodriguez, S., Baidoo, E.E., Keasling, J.D., 2009. Advances in analysis of microbial metabolic fluxes via (^{13})C isotopic labeling. Mass Spectrom. Rev. 28, 362–375.
Varma, A., Palsson, B.O., 1993. Metabolic capabilities of *Escherichia-Coli* .1. Synthesis of biosynthetic precursors and cofactors. J. Theor. Biol. 165, 477–502.
Varma, A., Palsson, B.O., 1994. Stoichiometric flux balance models quantitatively predict growth and metabolic by-product secretion in wild-type *Escherichia-Coli* W3110. Appl. Environ. Microbiol. 60, 3724–3731.
Vemuri, G.N., Altman, E., Sangurdekar, D.P., Khodursky, A.B., Eiteman, M.A., 2006. Overflow metabolism in *Escherichia coli* during steady-state growth: transcriptional regulation and effect of the redox ratio. Appl. Environ. Microbiol. 72, 3653–3661.
Wiechert, W., 2001. ^{13}C metabolic flux analysis. Metab. Eng. 3, 195–206.
Wiechert, W., 2002. Modeling and simulation: tools for metabolic engineering. J. Biotechnol. 94, 37–63.
Wiechert, W., de Graaf, A.A., 1997. Bidirectional reaction steps in metabolic networks: I. Modeling and simulation of carbon isotope labeling experiments. Biotechnol. Bioeng. 55, 101–117.
Wiechert, W., Mollney, M., Petersen, S., de Graaf, A.A., 2001. A universal framework for ^{13}C metabolic flux analysis. Metab. Eng. 3, 265–283.
Wiechert, W., Schweissgut, O., Takanaga, H., Frommer, W.B., 2007. Fluxomics: mass spectrometry versus quantitative imaging. Curr. Opinion Plant Biol. 10, 323–330.
Wiechert, W., Siefke, C., de Graaf, A.A., Marx, A., 1997. Bidirectional reaction steps in metabolic networks: II. Flux estimation and statistical analysis. Biotechnol. Bioeng. 55, 118–135.
Wittmann, C., 2002. Metabolic flux analysis using mass spectrometry. Adv. Biochem. Eng. Biotechnol. 74, 39–64.
Yoshida, A., Nishimura, T., Kawaguchi, H., Inui, M., Yukawa, H., 2005. Enhanced hydrogen production from formic acid by formate hydrogen lyase-overexpressing *Escherichia coli* strains. Appl. Environ. Microbiol. 71, 6762–6768.
Zamboni, N., Fendt, S.M., Ruhl, M., Sauer, U., 2009. (^{13})C-based metabolic flux analysis. Nat. Protocols 4, 878–892.
Zamboni, N., Fischer, E., Sauer, U., 2005. FiatFlux—a software for metabolic flux analysis from ^{13}C-glucose experiments. BMC Bioinformatics 6, 209.
Zhao, J., Shimizu, K., 2003. Metabolic flux analysis of *Escherichia coli* K12 grown on ^{13}C-labeled acetate and glucose using GC–MS and powerful flux calculation method. J. Biotechnol. 101, 101–117.